

The Cosmic Ray Energy Spectrum Measured with KASCADE-Grande

A. Haungs*, W.D. Apel*, J.C. Arteaga^{†,xi}, F. Badea*, K. Bekk*, M. Bertaina[‡], J. Blümer^{*,†}, H. Bozdog* I.M. Brancus[§], M. Brüggemann[¶], P. Buchholz[¶], E. Cantoni^{‡,||}, A. Chiavassa[‡], F. Cossavella[†], K. Daumiller*, V. de Souza^{†,xii}, F. Di Pierro[‡], P. Doll*, R. Engel*, J. Engler*, M. Finger*, D. Fuhrmann**, P.L. Ghia^{||}, H.J. Gils*, R. Glasstetter**, C. Grupen[¶], D. Heck*, J.R. Hörandel^{†,xiii}, T. Huege*, P.G. Isar*, K.-H. Kampert**, D. Kang[†], D. Kickelbick[¶], H.O. Klages*, P. Łuczak^{††}, H.J. Mathes*, H.J. Mayer*, J. Milke*, B. Mitrica[§], C. Morello^{||}, G. Navarra^{†,xv}, S. Nehls*, J. Oehlschläger*, S. Ostapchenko^{*,xiv}, S. Over[¶], M. Petcu[§], T. Pierog*, H. Rebel*, M. Roth*, H. Schieler*, F. Schröder*, O. Sima^{‡‡}, M. Stümpert[†], G. Toma[§], G.C. Trinchero^{||}, H. Ulrich*, A. Weindl*, J. Wochele*, M. Wommer*, J. Zabierowski^{††}

*Institut für Kernphysik, Karlsruher Institut für Technologie, 76021 Karlsruhe, Germany

[†]Institut für Experimentelle Kernphysik, Karlsruher Institut für Technologie, 76021 Karlsruhe, Germany

[‡]Dipartimento di Fisica Generale dell'Università, 10125 Torino, Italy

[§]National Institute of Physics and Nuclear Engineering, 7690 Bucharest, Romania

[¶]Fachbereich Physik, Universität Siegen, 57068 Siegen, Germany

^{||}Istituto di Fisica dello Spazio Interplanetario, INAF, 10133 Torino, Italy

**Fachbereich Physik, Universität Wuppertal, 42097 Wuppertal, Germany

^{††}Soltan Institute for Nuclear Studies, 90950 Lodz, Poland

^{‡‡}Department of Physics, University of Bucharest, 76900 Bucharest, Romania

^{xi}now at: Universidad Michoacana, Morelia, Mexico

^{xii}now at: Universidade de São Paulo, Instituto de Física de São Carlos, Brasil

^{xiii}now at: Dept. of Astrophysics, Radboud University Nijmegen, The Netherlands

^{xiv}now at: University of Trondheim, Norway

^{xv}This article is dedicated to Gianni Navarra, a principle investigator of KASCADE-Grande and an outstanding cosmic ray scientist, who passed away much too soon on August 24, 2009.

Abstract. KASCADE-Grande is a multi-detector experiment at Forschungszentrum Karlsruhe, Germany for measuring extensive air showers in the primary energy range of 100 TeV to 1 EeV. This contribution attempts to provide a synopsis of the current results of the experiment. In particular, the reconstruction of the all-particle energy spectrum in the range of 10 PeV to 1 EeV based on four different methods with partly different sources of systematic uncertainties is presented. Since the calibration of the observables in terms of the primary energy and mass depends on Monte Carlo simulations, we compare the results of various methods applied to the same sample of measured data. In addition, first investigations on the elemental composition of the cosmic particles as well as on tests of hadronic interaction models underlying the analyses are discussed.

Keywords: High-energy cosmic rays, extensive air showers, KASCADE-Grande

I. INTRODUCTION

The main goal of experimental cosmic ray research is the measurement of the primary energy spectrum and the elemental composition. That comprises important hints to understand the origin, acceleration and propagation of energetic cosmic particles. This task can be done

directly or indirectly, depending on the energy of the primary particle. At high energies, above 10^{15} eV the energy spectrum must be determined indirectly from the measured properties of extensive air showers (EAS) that cosmic rays induce in the Earth's atmosphere.

Depending on the experimental apparatus and the detection technique, different sets of EAS observables are available to estimate the energy of the primary cosmic ray [1]. In ground arrays the total number of charged particles in the shower and the corresponding density at observation level are commonly employed [2]. However, the muon content of EAS can play also an important role. One reason in favor of this observable is that in an air shower muons undergo fewer atmospheric interactions than the electromagnetic or hadronic components (dominant component for vertical EAS) and exhibit in consequence less fluctuation compared to the more abundant electromagnetic component.

In KASCADE-Grande both components, the muon and the electromagnetic are measured and both, together with their correlation on a single-event-basis are used to derive the energy spectrum and composition of cosmic rays in the range from 10^{16} to 10^{18} eV.

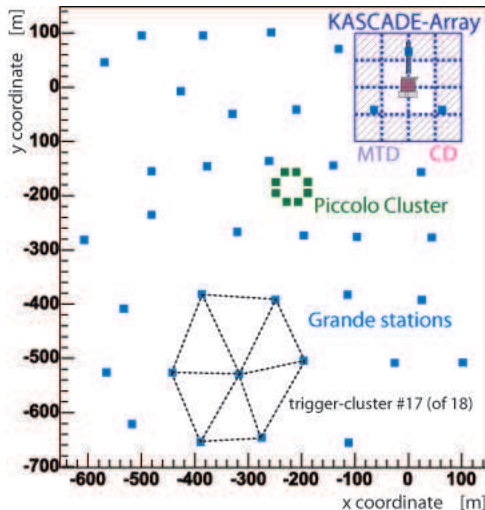


Fig. 1: Layout of the KASCADE-Grande experiment: The original KASCADE, the distribution of the 37 stations of the Grande array, and the small Piccolo cluster for fast trigger purposes are shown. The outer 12 clusters of the KASCADE array consist of μ - and e/γ -detectors, the inner 4 clusters of e/γ -detectors only.

II. KASCADE-GRANDE

Main parts of the experiment are the Grande array spread over an area of $700 \times 700 \text{ m}^2$, the original KASCADE array covering $200 \times 200 \text{ m}^2$ with unshielded and shielded detectors, and additional muon tracking devices. This multi-detector system allows us to investigate the energy spectrum, composition, and anisotropies of cosmic rays in the energy range up to 1 EeV . The estimation of energy and mass of the primary particles is based on the combined investigation of the charged particle, the electron, and the muon components measured by the detector arrays of Grande and KASCADE.

The multi-detector experiment KASCADE [3] (located at 49.1°N , 8.4°E , 110 m.a.s.l.) was extended to KASCADE-Grande in 2003 by installing a large array of 37 stations consisting of 10 m^2 scintillation detectors each (fig. 1). KASCADE-Grande [4] provides a sensitive area of $\approx 0.4 \text{ km}^2$ and operates jointly with the existing KASCADE detectors. The joint measurements with the KASCADE muon tracking devices are ensured by an additional cluster (Piccolo) close to the center of KASCADE-Grande for fast trigger purposes.

While the Grande detectors are sensitive to charged particles, the KASCADE array detectors measure the electromagnetic component and the muonic component separately. The muon detectors enable to reconstruct the total number of muons on an event-by-event basis also for Grande triggered events. The Muon Tracking Detector (MTD) [5] registers muons above an energy threshold of 800 MeV . At the MTD the directions of muon tracks in EAS are measured with an excellent angular resolution of $\approx 0.35^\circ$. These directional data allow to investigate the longitudinal development of

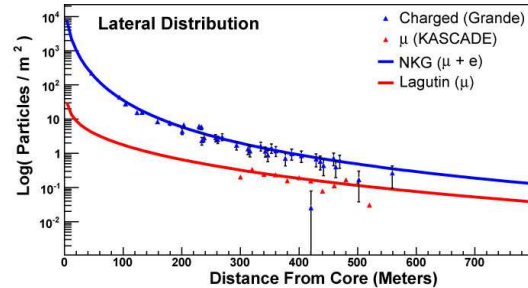


Fig. 2: Example of a typical KASCADE-Grande event. Displayed are the measured densities per station for charged particles of the Grande array and averaged over stations in 20 m rings for the KASCADE muon array, respectively and the corresponding fits of the lateral distribution functions.

the muonic component in showers which is used as a signature of the development of the hadronic EAS core.

III. RECONSTRUCTION

Basic shower observables like the core position, angle-of-incidence, and total number of charged particles are provided by the measurements of the Grande stations. By means of Monte Carlo simulations a core position resolution of $\approx 5 \text{ m}$, a direction resolution of $\approx 0.7^\circ$, and a resolution of the total particle number in the showers of $\approx 15\%$ is expected [6]. The total number of muons (N_μ resolution $\approx 25\%$) is calculated using the core position determined by the Grande array and the muon densities measured by the KASCADE muon array detectors [7]. Fig. 2 shows a typical event of KASCADE-Grande and its reconstruction; i.e. the functions fitted to the measured lateral particle density distributions. Full efficiency for triggering and reconstruction of air-showers is reached at primary energy of $\approx 2 \cdot 10^{16} \text{ eV}$, slightly depending on the cuts needed for the reconstruction of the different observables.

For a subsample of events collected by the Grande array it is possible to compare on an event-by-event basis the two independent reconstructions of KASCADE and Grande. This provides the unique opportunity of evaluating the reconstruction accuracies of the Grande array by a direct comparison with an independent experiment. Since the KASCADE array is much more dense, the values of reconstructed observables from KASCADE are taken as reference. The subsample is obtained accordingly to the following selection criteria: maximum energy deposit in one of the Grande stations close to KASCADE; core position within a circle of 90 m radius from the KASCADE center; zenith angle less than 40° . By means of such a comparison (see fig. 3) the Grande reconstruction accuracies are found to be for the shower size: systematic uncertainty $\leq 5\%$, statistical inaccuracy $\leq 15\%$; for arrival direction: $\sigma \approx 0.6^\circ$; for the core position: $\sigma \approx 5 \text{ m}$. All of them are in good accordance with the resolutions obtained from simulations.

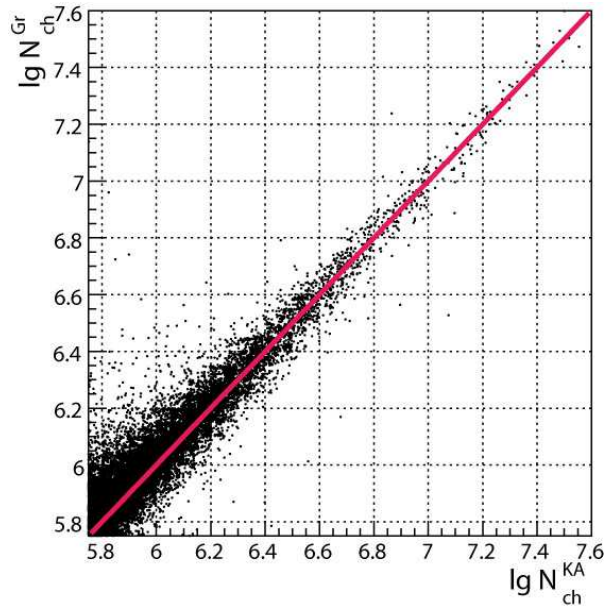


Fig. 3: Scatter plot of the shower sizes (charged particles) reconstructed by KASCADE (x-axis) and Grande (y-axis).

IV. ALL-PARTICLE ENERGY SPECTRUM

A. Strategy

Applying different methods to the same data sample has advantages in various aspects: one would expect the same result for the energy spectrum by all methods provided the measurements are accurate enough, when the reconstructions work without failures, and when the Monte Carlo simulations describe correctly the shower development. But, the fact that the various observables exhibit substantial differences in their composition sensitivity hampers a straightforward analysis. However, investigating results of different methods can be used to

- cross-check the measurements by different sub-detectors;
- cross-check the reconstruction procedures;
- cross-check the influence of systematic uncertainties;
- test the sensitivity of the observables to the elemental composition;
- test the validity of hadronic interaction models underlying the simulations.

B. Methods

The estimation of the all-particle energy spectrum is presently based on four different methods using different observables of KASCADE-Grande:

- N_{ch} -method: The reconstructed charged particle shower size per individual event is corrected for attenuation in the atmosphere by the constant intensity cut method and calibrated by Monte Carlo simulations under the assumption of a dependence

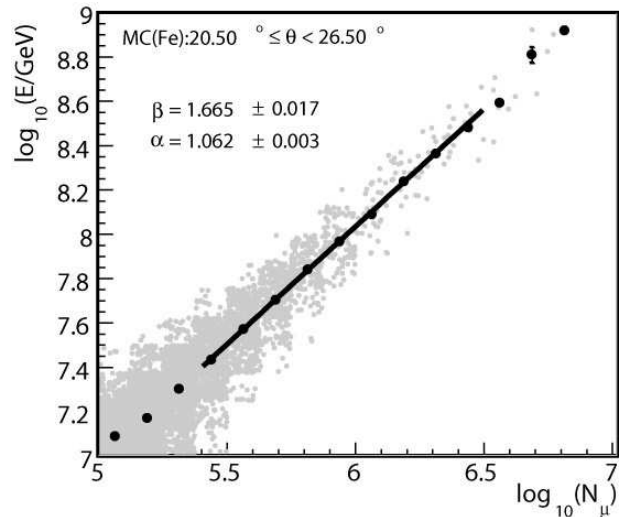


Fig. 4: Mean distribution of true energy vs. muon number for iron nuclei and $\theta = 20.5^\circ - 26.5^\circ$ calculated with MC simulations. The fit with formula $E[\text{GeV}] = \beta \cdot N_\mu^\alpha$ is shown.

$E_0 \propto N_{ch}^{\alpha_{ch}}$ and a particular primary composition [8].

- N_μ -method: The reconstructed muon shower size per individual event is corrected for attenuation and calibrated by Monte Carlo simulations under the assumption of a dependence $E_0 \propto N_\mu^{\alpha_\mu}$ (see example in fig. 4) and a particular primary composition [9].
- $N_{ch} - N_\mu$ -method: This method combines the information provided by the two observables. By help of Monte Carlo simulations a formula is obtained to calculate the primary energy per individual shower on basis of N_{ch} and N_μ . The formula takes into account the mass sensitivity in order to minimize the composition dependence. The attenuation is corrected for by deriving the formula for different zenith angle intervals independently and combining the energy spectrum afterwards [10].
- $S(500)$ -method: The reconstructed particle density at the specific distance to the shower axis of 500 m per individual event is corrected for attenuation and calibrated by Monte Carlo simulations under the assumption of a dependence $E_0 \propto S(500)^{\alpha_{S(500)}}$. The distance of 500 m is chosen to have a minimum influence of the primary particle type, therefore a smaller dependence on primary composition is expected [11].

In figure 5 the resulting spectra are compiled. Owing to the different procedures, the results for the first two methods are shown under proton and iron assumption, respectively, only, whereas for the other two methods the resulting all-particle energy spectra are displayed. Figure 6 shows the same results but with the flux multiplied by a factor of $E^{3.0}$.

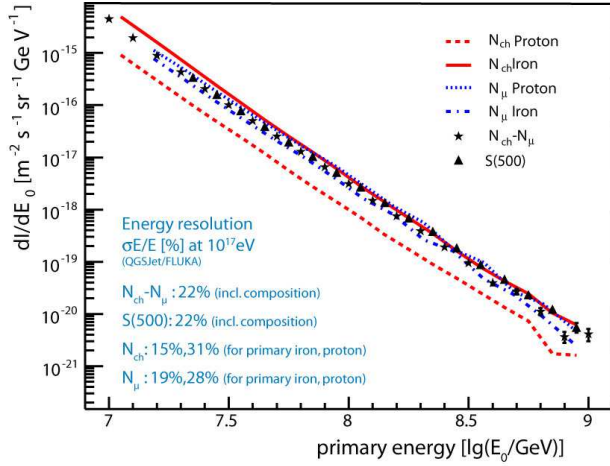


Fig. 5: Reconstructed all-particle energy spectrum by four different methods applied to KASCADE-Grande data. Given are also the energy resolutions for the methods.

C. Systematic uncertainties and attenuation

The application of the different methods allows us to compare and cross-check the influence of various sources of systematic uncertainties. The N_{ch} -method uses the basic measurements of the Grande array only, resulting in a high accuracy of N_{ch} with better than 15% over the whole range of shower size, without any energy dependent bias. But, using only one observable, there is a large dependence on the primary elemental composition, reflected by the distance between the spectra obtained for proton and iron assumption at the calibration. The N_{μ} -method on the other hand is based on the muon shower size, which can be derived less accurately (25% with a small bias dependent on the distance of the shower core to the muon detectors which is corrected for), but with much less composition dependence. The N_{ch} - N_{μ} -method, owing to the combination of the reconstruction uncertainty of two variables, shows basically a larger uncertainty in the reconstruction, but this is compensated by taking into account the correlation of these observables at individual events. Furthermore, by this procedure the composition dependence is strikingly decreased. The $S(500)$ value by construction yields a larger uncertainty of the variable reconstruction, but has also a minor composition dependence.

For all methods, the energy resolution is estimated using full Monte Carlo simulations and comparing the reconstructed with the simulated primary energy (for instance figure 5 gives the numbers for an energy of $E_0 = 10^{17}$ eV). Values of systematic uncertainties in the flux determination for the different methods are shown in fig. 6 (again for $E_0 = 10^{17}$ eV). To a large amount these uncertainties are due to the reconstruction of the observables, but there are additional sources of systematics which belong to all methods: e.g., concerning the Monte Carlo statistics, the assumed Monte Carlo spectral slope, or the fits of the calibration procedures. The different

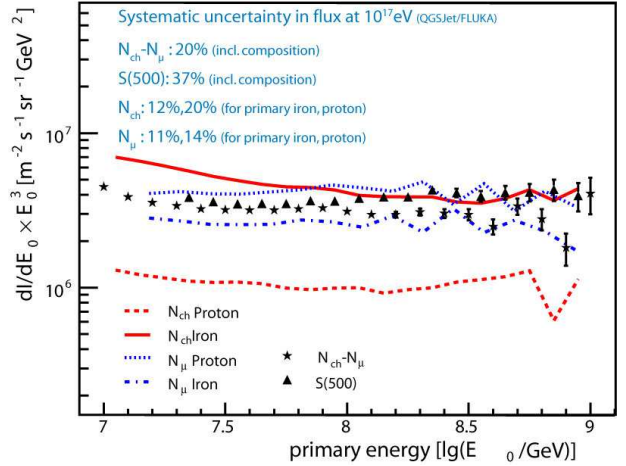


Fig. 6: Same as figure 5, but the flux multiplied by E_0^3 . Values for the uncertainty in the flux determination are given for the different methods.

attenuation (and its handling to correct for) of the various observables ($\Lambda(N_{ch}) \approx 495 \pm 20$ g/cm²; $\Lambda(N_{\mu}) \approx 1100 \pm 100$ g/cm²; $\Lambda(S(500)) \approx 347 \pm 22$ g/cm² at $E_0 = 10^{17}$ eV) however, lead again to slightly different contributions to the total systematic uncertainty. The total uncertainties (energy resolution and systematics) for the various methods are discussed in refs. [8], [9], [10], [11] and can be displayed as a band surrounding the reconstructed energy spectrum (e.g., see fig. 9).

D. Discussion

Taking into account the systematic uncertainties, there is a fair agreement between the all-particle energy spectra of the different applications (fig. 6).

Of particular interest is the fact that by using N_{ch} , the iron assumption predicts a higher flux than the proton assumption, whereas using N_{μ} the opposite is the case. That means that the ‘true spectrum has to be a solution inside the range spanned by the two methods. If there is only the possibility of applying one method, then there is a large variance in possible solutions (everything within the range spanned by proton and iron line, not even parallel to these lines). However, more detailed investigations have shown, that a structure in the spectrum or a sudden change in composition would be retained in the resulting spectrum, even if the calibration is performed with an individual primary, only. Interestingly, over the whole energy range there is only little room for a solution satisfying both ranges, spanned by N_{ch} and N_{μ} , and this solution has to be of relatively heavy composition - in the framework of the QGSJet-II hadronic interaction model. The narrower range for a solution provided by the N_{μ} -method compared to N_{ch} confirms the finding of KASCADE that at sea-level the number of mostly low-energy muons N_{μ} is a very good and composition insensitive energy estimator.

The results of the composition independent N_{ch} - N_{μ} -, and $S(500)$ -methods lie inside the area spanned

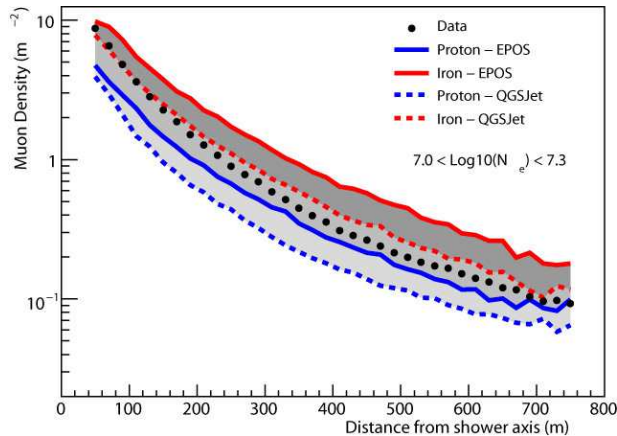


Fig. 7: Lateral distribution of muons compared to the predictions of QGSJet-II and EPOS 1.61.

by the composition dependent methods, which is a very promising result. The $S(500)$ -method results in a slightly higher flux than the $N_{ch}-N_{\mu}$ -method, but the two spectra are consistent taking into account the systematic uncertainties.

All the discussed results show a smooth all-particle energy spectrum without a clear hint to a distinct structure over the whole energy range from 10 PeV to 1 EeV. Another conclusion is that, taking into account the systematic uncertainties for all methods, the underlying hadronic interaction model (QGSJet-II/FLUKA) is intrinsically consistent, i.e. the correlation between the different observables, respectively the particle components can describe the global features of our measurements.

V. HADRONIC INTERACTION MODELS

By now, for all the considerations the models QGSJet-II and FLUKA [12], [13], [14] have been used, only. Other interaction models would probably change the interpretation of the data. In the following it is briefly described how we investigate the influence of hadronic interaction models on the interpretation of the measured data.

A. Muon densities

Local muon densities measured with the KASCADE array are studied in their correlation with distance from the shower axis and the total number of electrons in the shower [15].

Figure 7 shows the mean muon density as a function of the distance from the shower axis compared to the predictions of QGSJet-II and EPOS 1.61. Both hadronic interaction models include the data within the proton and iron limits for the entire range of distances from 100 to 750 meters. Not only the absolute density but also the slope of the LDF is of interest for checking the validity of hadronic interaction models. Considering an equal probability trigger for protons and iron primaries as a function of distance from the shower axis, one should expect the measured LDF to be parallel to

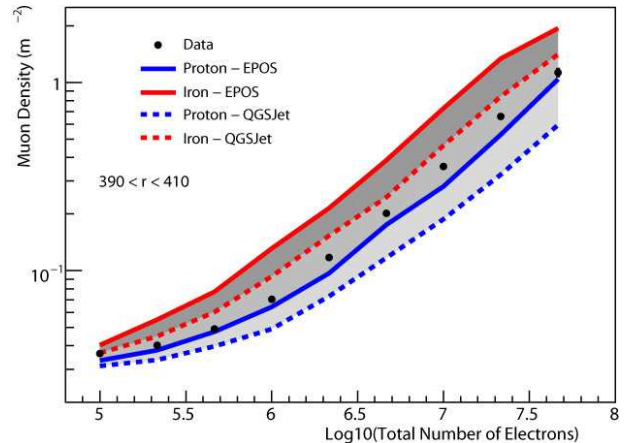


Fig. 8: Muon density as a function of the total number of electrons compared to the predictions of QGSJet-II and EPOS 1.61.

primaries of pure composition. Note that the LDFs of simulated proton and iron showers are parallel. However the measured LDF is neither parallel to the QGSJet-II nor to the EPOS 1.61 curves. It shows that the slope of the LDF cannot be well described by either model.

Figure 8 shows the evolution of the mean muon density as a function of N_e . The calculations done with QGSJet-II and EPOS 1.61 using proton and iron nuclei as primary particles embrace the data in the entire range of $5 < \lg(N_e) < 8$.

Nevertheless, both figures 7 and 8 show that EPOS 1.61 would require a very light primary composition in order to fit the data. On the other hand, QGSJet-II could fit the data with an intermediate primary abundance between proton and iron nuclei.

B. All-particle energy spectrum

To study effects on the all-particle energy spectrum we investigated the influence of the hadronic interaction model exemplary by performing the N_{ch} -method based on simulations with the hadronic interaction model EPOS vers.1.61 [16] in addition to QGSJet-II. As the Monte Carlo statistics is limited in case of EPOS, both spectra were obtained by generating the calibration curve with an equally mixed composition of five primaries (H,He,C,Si,Fe). Figure 9 compares the all-particle energy spectrum obtained with the KASCADE-Grande data set for both cases. The interpretation of the KASCADE-Grande data with EPOS leads to a significantly higher flux compared to the QGSJet-II result. Though we know, that version 1.61 of the EPOS model is not fully consistent with air shower data (in particular, it cannot describe the correlation of hadronic observables with the muon and electron content of the EAS [17]) this example shows that applying and comparing various reconstruction methods on the same data set will be useful for a better understanding of the interaction processes in the air shower development.

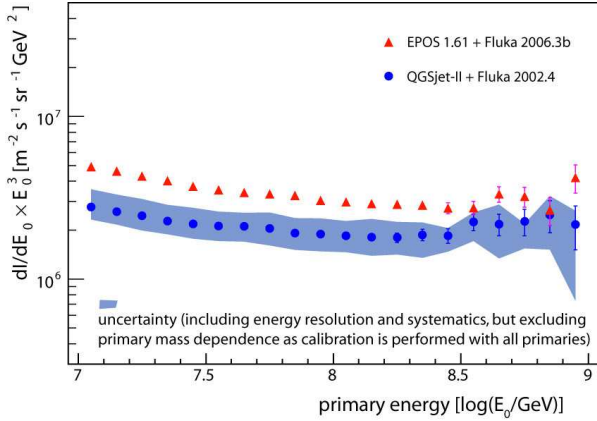


Fig. 9: Reconstructed all-particle energy spectrum with the N_{ch} -method and the calibration function obtained by assuming mixed composition, but based on two different hadronic interaction models.

C. Muon Tracking Detector

More general investigations of the characteristics of the hadronic interaction models are provided by studies of the muon tracking data [18]. Main observables of interest are the mean muon radial angles and the mean muon pseudo-rapidities [19], which are reconstructed in a given distance range from the shower core, and which are quantities sensitive to the development of the extensive air shower. Vertical showers ($\theta \leq 18^\circ$) with size $\lg N_e > 6$ have been selected. The lateral distributions of those two quantities have been obtained and compared with the results reconstructed out of the simulated data for two primary species: proton and iron. The simulations were done with CORSIKA [12] code using the QGSJet-II model [13] for high energy interactions above 200 GeV and FLUKA2006 [14] below that energy. The comparisons are done in limited ranges of muon distances to the core, where the saturation effects (seen below 150 m) and trigger inefficiencies (seen above 400 m) are not present. For the mean radial angle (fig. 10) we can conclude that the experimental data are compatible with the CORSIKA simulations using the QGSJet-II - FLUKA model combination, as the data points are in between the simulated ones. The lines are linear fits to the simulation results. The error bars in the simulations are still very large and the number of simulated data will be increased, thus the results are marked as preliminary. We also notice that the experimental data tend to be positioned closer to the line of iron initiated showers rather than proton ones, like for the muon densities shown in fig. 7. In fig. 11, where lateral distributions of the mean muon pseudorapidity for the same data set are compared, one can also conclude that the experimental data points are bracketed by the simulated distributions, however, the data points here are closer to the proton simulation results. This inconsistency may be an indication of the features of the models. The mean radial angle distribution suggests that

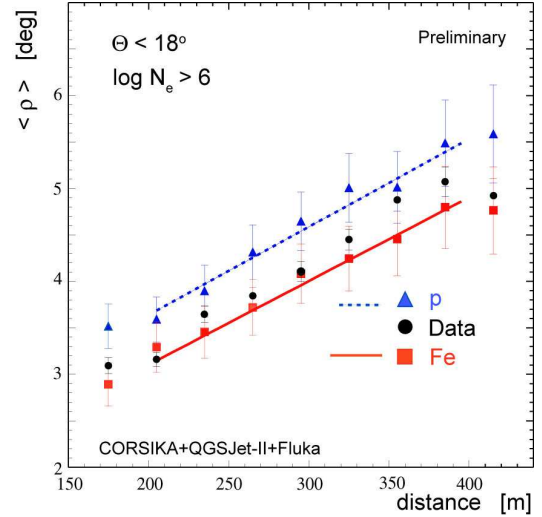


Fig. 10: Reconstructed lateral distribution of the mean radial angle compared with CORSIKA simulation results for proton and iron primaries. Lines are fits to the simulations.

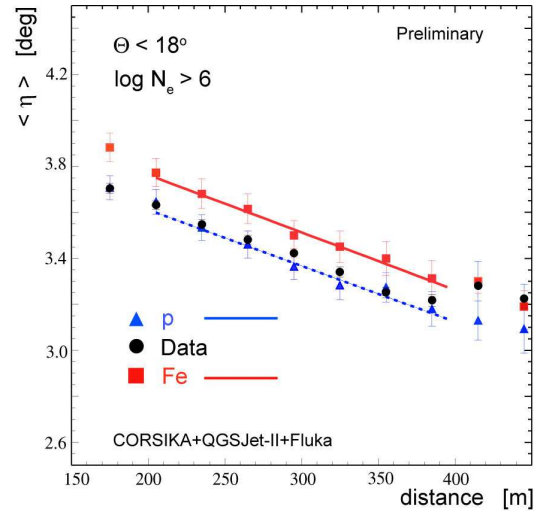


Fig. 11: Reconstructed lateral distribution of the mean muon pseudorapidity compared with CORSIKA simulation results for proton and iron primaries. Lines are fits to the simulations.

the transverse momentum of pions produced in hadronic interactions is reproduced by the models, but fig. 11 is a hint that the simulations provide relatively more high rapidity pions.

VI. COMPOSITION

The basic goal of the KASCADE-Grande experiment is the determination of the chemical composition in the primary energy range $10^{16} - 10^{18}$ eV. Like for the reconstruction of the energy, again several methods using different observables will be applied to the registered data, in order to study systematic uncertainties. However, the influence of predictions of the hadronic interaction models has a much larger influence on the composi-

tion than compared to the primary energy. The main observables taken into account for composition studies at KASCADE-Grande are the shower size (N_e) and muon size (N_μ). For all the methods it is crucial to verify the sensitivity of the observables to different primary particles and the reproducibility of the measurements with the hadronic interaction model in use as a function of sizes and the atmospheric depth. Two examples how we approach the composition studies are discussed in the following:

A. Muon densities

In addition to the validity checks of the hadronic interaction models the reconstruction of the local muon density at a certain distance to the shower core gives a sensitivity to changes in the elemental composition [15] (see figs. 7 and 8). The data as shown in figure 8 can be used to study a possible transition of the primary composition with increasing total number of electrons, but conclusive results are presently not possible due to the strong dependence on the hadronic interaction model. However, the analysis done with both models show no abrupt change in the composition in the entire energy range. EPOS 1.61 would require a very light abundance of primary particles in order to fit the data. QGSJet-II could fit the data with an intermediate primary abundance. The change in slope seen in figure 8 for $\log_{10}(N_e) < 6.0$ corresponds to the threshold of the experiment and the fact that both data and simulation show the same behavior illustrates the good level of understanding of our detector.

B. Electron-muon number ratio

In the second example, the total number of electrons N_e and the total number of muons N_μ of each recorded event are considered and the distribution of N_μ/N_e is studied in different intervals of N_e (corresponding to different energy intervals) and zenith angle [20].

KASCADE-Grande data are chosen, at first, in an electron size range providing full reconstruction efficiency and high statistics: $6.5 \leq \log_{10}(N_e) < 6.75$ in $0^\circ \leq \theta < 24^\circ$ (equivalent to a primary energy just below 10^{17} eV). The same event selection is made on the simulated QGSJet-II data sets at disposal for each cosmic ray primary (p, He, C, Si, Fe) simulated with an energy spectrum with slope $\gamma = -3$. The experimental distribution of the observable N_μ/N_e is taken into account and fitted with a linear combination of elemental contributions from simulations. By this way the mean and the width of the distributions are taken into account.

It was found that by using only two primary masses for the fit, the measured distributions can not be described. Fig. 12 shows the fit performed with a combination of three elements: Protons, carbon and iron which is matching the light elements with the heaviest element. It can be seen that a three elements combination is well fitting the data, but it is also possible to use another

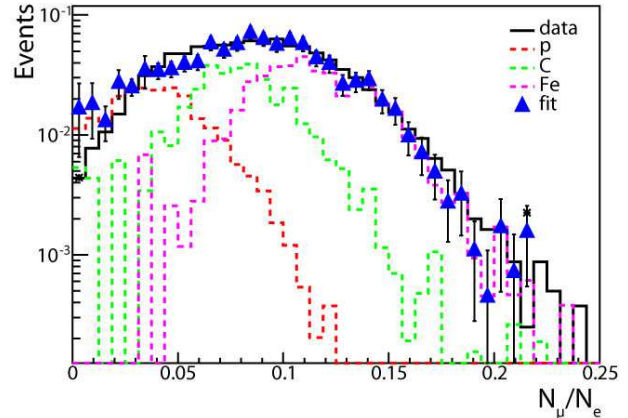


Fig. 12: The KASCADE-Grande data in $6.5 \leq \lg(N_e) < 6.75$ ($0^\circ \leq \theta < 24^\circ$) described by Protons, Carbon and Iron primaries.

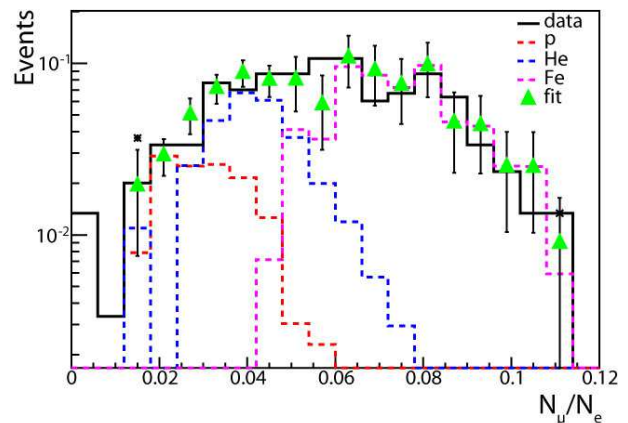


Fig. 13: The KASCADE-Grande data in $7.25 \leq \lg(N_e) < 7.5$ ($0^\circ \leq \theta < 24^\circ$) described by Protons, Helium and Iron primaries.

combination of primaries, e.g. protons, helium and iron. However, protons and iron primaries are needed to describe the edges and the width of the data distribution. These results show that the QGSJet model describes well the shape and the tails of the experimental distribution. Selecting the KASCADE-Grande experimental data for higher values of the electron size N_e means to choose showers that were generated by higher energy events (fig. 13 is for energies slightly above 10^{17} eV). Also in this case (as well as for other ranges in zenith angle), it is found that the model reproduces the data and the minimization of the N_μ/N_e distribution with three chemical components still provides a good result.

Summarizing, by such first composition studies it is seen that, by exploiting a chi-square minimization of a linear combination of different simulated primaries, the KASCADE-Grande N_μ/N_e distributions can only be fitted using at least three primary elements. QGSJet-II, the hadronic interaction model in use, can fairly well reproduce the data and, in particular, the tails of the distributions, that represent a main constraint being related to the lightest and heaviest cosmic ray primaries.

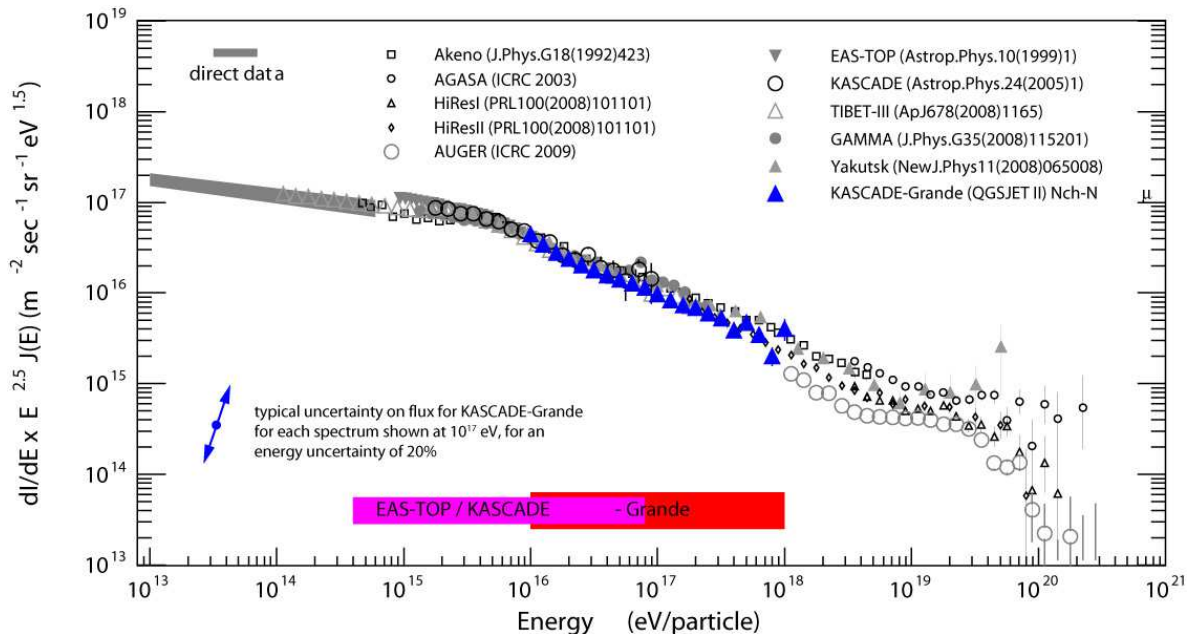


Fig. 14: Comparison of the all-particle energy spectrum obtained with KASCADE-Grande data to results of other experiments.

One has to remark, that using another hadronic interaction model would of course lead to significant changes in the relative abundances of the elemental groups as different models predict different means. But, as the width of the distributions are more or less independent of the interaction model, the fact that at least three primary mass groups are needed to describe the data is valid.

VII. CONCLUSIONS

Applying various different reconstruction methods to the KASCADE-Grande data the obtained all-particle energy spectra are compared for cross-checks of reconstruction, for studies of systematic uncertainties and for testing the validity of the underlying hadronic interaction models. The resulting energy spectra are consistent and in the overlapping energy range in a very good agreement to the spectrum obtained by the KASCADE, EAS-TOP, and other experiments (fig. 14). A wealth of information on individual showers is available with KASCADE-Grande. This makes it possible to reconstruct the all-particle energy spectrum with high precision, as well as to investigate the elemental composition, to test the hadronic interaction models, and to study cosmic ray anisotropies. All these studies are under way and results are expected in near future.

VIII. ACKNOWLEDGEMENTS

The KASCADE-Grande collaboration acknowledges the possibility to present their first results in a highlight talk at the 31st ICRC. KASCADE-Grande is supported by the BMBF of Germany, the MIUR and INAF of Italy, the Polish Ministry of Science and Higher Education (grant for 2009-2011), and the Romanian Ministry of Education, Research and Innovation (grant 461/2009).

This work was supported in part by the German-Polish bilateral collaboration grant (PPP - DAAD) for the years 2009-2010.

REFERENCES

- [1] A. Haungs, H. Rebel, M. Roth, Rep. Prog. Phys. 66 (2003) 1145.
- [2] M. Nagano and A.A. Watson., Rev. Mod. Phys. 72 (2000) 689.
- [3] T. Antoni et al - KASCADE Coll., Nucl. Instr. and Meth. A 513 (2003) 490.
- [4] A. Chiavassa et al. - KASCADE-Grande Coll., Proc. 21st Europ. Cosmic Ray Symp., Kosice, Slovakia (2008), published by Inst. of Physics, Slovak Academy of Sciences (2009) 521.
- [5] P. Doll et al., Nucl. Instr. and Meth. A 488 (2002) 517.
- [6] F. Di Piero et al. - KASCADE-Grande Coll., Proc. 31th ICRC, Lodz (Poland) 2009, #icrc0895.
- [7] D. Fuhrmann et al. - KASCADE-Grande Coll., Proc. 31th ICRC, Lodz (Poland) 2009, #icrc0131.
- [8] D. Kang et al. - KASCADE-Grande Coll., Proc. 31th ICRC, Lodz (Poland) 2009, #icrc1044.
- [9] J.C. Arteaga et al. - KASCADE-Grande Coll., Proc. 31th ICRC, Lodz (Poland) 2009, #icrc0805.
- [10] M. Bertaina et al. - KASCADE-Grande Coll., Proc. 31th ICRC, Lodz (Poland) 2009, #icrc0323.
- [11] G. Toma et al. - KASCADE-Grande Coll., Proc. 31th ICRC, Lodz (Poland) 2009, #icrc0347.
- [12] D. Heck et al., Report FZKA 6019, Forschungszentrum Karlsruhe (1998).
- [13] S.S. Ostapchenko, Nucl. Phys. B (Proc. Suppl.) 151 (2006) 143&147; S.S. Ostapchenko, Phys. Rev. D 74 (2006) 014026.
- [14] A. Fassò et al., Report CERN-2005-10, INFN/TC-05/11, SLAC-R-773 (2005).
- [15] V. de Souza et al. - KASCADE-Grande Coll., Proc. 31th ICRC, Lodz (Poland) 2009, #icrc0499.
- [16] K. Werner, F.M. Liu, T. Pierog, Phys. Rev. C 74 (2006) 044902.
- [17] W.D. Apel et al. - KASCADE-Grande Coll., J. Phys. G: Nucl. Part. Phys. 36 (2009) 035201.
- [18] P. Doll et al. - KASCADE-Grande Coll., Proc. 31th ICRC, Lodz (Poland) 2009, #icrc0429.
- [19] J. Zabierowski et al. - KASCADE-Grande Coll., Proc. 31th ICRC, Lodz (Poland) 2009, #icrc0171.
- [20] E. Cantoni et al. - KASCADE-Grande Coll., Proc. 31th ICRC, Lodz (Poland) 2009, #icrc0524.